Available online at www.sciencedirect.com
ScienceDirect
International Journal of Heat and Fluid Flow 28 (2007) 1280–1290
International Journal of HEAT AND FLUID FLOW
www.elsevier.com/locate/ijhff

Coherent fine scale eddies in turbulence transition of spatially-developing mixing layer

Y. Wang *, M. Tanahashi, T. Miyauchi

Department of Mechanical and Aerospace Engineering, Tokyo Institute of Technology, 2-12-1 Ookayama, Meguro-ku, Tokyo 152-8550, Japan

Received 7 February 2007; received in revised form 28 June 2007; accepted 29 June 2007
Available online 24 August 2007

Abstract

To investigate the relationship between characteristics of the coherent fine scale eddy and a laminar–turbulent transition, a direct numerical simulation (DNS) of a spatially-developing turbulent mixing layer with $Re_{\omega,0} = 700$ was conducted. On the onset of the transition, strong coherent fine scale eddies appears in the mixing layer. The most expected value of maximum azimuthal velocity of the eddy is 2.0 times Kolmogorov velocity (u_k), and decreases to $1.2u_k$, which is an asymptotic value in the fully-developed state, through the transition. The energy dissipation rate around the eddy is twice as high compared with that in the fully-developed state. However, the most expected diameter and eigenvalues ratio of strain rate acting on the coherent fine scale eddy are maintained to be 8 times Kolmogorov length (η) and $\alpha{:}\beta{:}\gamma = -5{:}1{:}4$ in the transition process. In addition to Kelvin–Helmholtz rollers, rib structures do not disappear in the transition process and are composed of lots of coherent fine scale eddies in the fully-developed state instead of a single eddy observed in early stage of the transition or in laminar flow.

Keywords: Laminar–turbulent transition; Turbulent mixing layer; Direct numerical simulation; Coherent fine scale eddy

1. Introduction

With the transition to turbulence, fine scale eddies can be observed in turbulent mixing layers (Moser and Rogers, 1991; Comte et al., 1992; Moser and Rogers, 1993; Rogers and Moser, 1994). Visualizations of flow field have shown that the fine scale eddies have a tube-like feature and the energy dissipation rate around them is high (Tanahashi and Miyauchi, 1995; Tanahashi et al., 1997a). This tube-like feature of fine scale motion in turbulent mixing layers recalls the tube-like structures observed in homogeneous turbulence (She et al., 1990; Vincent and Meneguzzi, 1991; Jimenez et al., 1993), which are considered as the smallest structure related to the intermittency of turbulence. Since lack of the knowledge about the fine scale motions of turbulence phenomena prevents the development of a proper turbulence theory and turbulence model, the fine scale structure of turbulence has been considered as one of the most important subjects in turbulence research. In the theories of small-scale structure, tube-like or sheet-like vortices have been considered as the smallest structures in turbulence (Townsend, 1951; Tennekes, 1968; Lundgren, 1982; Pullin and Saffman, 1993).

In our previous studies (Tanahashi et al., 1996, 1997b), we have identified cross-sections perpendicular to rotation axis of tube-like eddies in homogeneous isotropic turbulence, and have shown that the most expected diameter of these eddies is about eight times Kolmogorov length (η) and the most expected maximum azimuthal velocity is about 1.2 times Kolmogorov velocity (u_k). Note that, it has been reported that the maximum azimuthal velocity can be scaled by $0.5u_{\mathrm{rms}}$ in low Reynolds number cases due to the deficient scale separation between u_k and u_{rms}. Recent analyses for higher Reynolds number cases has shown that the maximum azimuthal velocity is scaled by

* Corresponding author. Tel./fax: +81 3 5734 2505.
E-mail address: wang@navier.mes.titech.ac.jp (Y. Wang).

0142-727X/$ - see front matter © 2007 Elsevier Inc. All rights reserved.
doi:10.1016/j.ijheatfluidflow.2007.06.009

u_k (Tanahashi et al., 2004). These tube-like eddies have also been found in other kinds of turbulent flows such as turbulent mixing layers (Tanahashi et al., 2001) and turbulent channel flows (Tanahashi et al., 2004). All these fine scale eddies show similar characteristics and weak Reynolds number dependence. Therefore, the tube-like eddy is called as a "coherent fine scale eddy" and is considered as a universal structure in the complicated turbulent flows.

Characteristics of the coherent fine scale eddy in fully-developed turbulent flows have been clarified in our previous researches (Tanahashi et al., 2001, 2004). Coherent fine scale eddies appearing in the laminar–turbulent transition have been studied by using DNS data of a temporally-developing mixing layer (Tanahashi et al., 1997a). However, to investigate the laminar–turbulent transition in more detail, analyses of spatially-developing flows, which include feedback interactions between upstream and downstream, are required. Because the spatially-developing mixing layer does not adopt a periodic assumption in the streamwise direction, it could be an exact description of the mixing layer used in many applications. However, it has been very difficult to set up proper inflow–outflow boundary conditions and requirements for the computer resources such as memories and CPU time have been an overabundance for the computers. Due to these problems, most of the researches on the mixing layer were conducted by using a temporally-developing mixing layer. It should be noted that, without the feedback interactions, the transition process would not be reproduced exactly.

In this study, DNS of a spatially-developing turbulent mixing layer with relatively high Reynolds number is conducted and relations between the coherent fine scale eddy and the laminar–turbulent transition are investigated.

2. Direct numerical simulation of a spatially-developing mixing layer

In this study, DNS of a spatially-developing turbulent mixing layer was conducted by solving incompressible Navier–Stokes equations and continuity equation:

$$\frac{\partial \boldsymbol{u}}{\partial t} + \boldsymbol{u}\cdot(\nabla \boldsymbol{u}) = -\nabla p + \frac{1}{Re_{\omega,0}}\nabla^2 \boldsymbol{u}, \tag{1}$$

$$\nabla \cdot \boldsymbol{u} = 0. \tag{2}$$

These equations are non-dimensionalized by the mean velocity difference ($\Delta U = U_1 - U_2$) and the vorticity thickness ($\delta_{\omega,0}$) at the inlet which is defined as follows:

$$\delta_{\omega,0} = \frac{\Delta U}{(\partial U(y)/\partial y)_{\max}}, \tag{3}$$

where $U(y)$ is the mean streamwise velocity at the inlet.

In the streamwise direction, finite difference methods with high accuracy are used for the discretization. For the pressure terms and viscous terms, fourth-order central difference method is utilized. For the convective terms, a special upwind scheme; "a localized upwind scheme" (Miyauchi et al., 1996), is used and its accuracy is fifth order. By using this scheme, instabilities caused by the numerical errors of finite difference methods and aliasing errors will be controlled by effects of the numerical viscosity. Simultaneously, it will be prevented effectively that the numerical viscosity would act too much if there is a mean flow in the flow field such as a mixing layer. All variables are expanded by sine/cosine series in the transverse direction with free slip boundary conditions, and by Fourier series in the spanwise direction with periodic boundary conditions. In the transverse and spanwise directions, aliasing errors from non-linear terms in the governing equation are fully removed by a 3/2 rule. In the streamwise direction, by using "the localized upwind scheme", aliasing errors can be suppressed to be small. The time integration is conducted by second-order Adams–Bashforth scheme for the convective and viscous terms, and by first-order backward-Euler scheme for the pressure term.

The mean velocity distribution at the inlet is given by a hyperbolic tangent velocity profile. Here, effects of the wake from the splitter plate are neglected. Three-dimensional random perturbations (u', v', w') are superposed on the mean velocity:

$$u(0,y,z,t) = U_m + 0.5\tanh(2y) + u'(y,z,t), \tag{4}$$

$$v(0,y,z,t) = v'(y,z,t), \tag{5}$$

$$w(0,y,z,t) = w'(y,z,t), \tag{6}$$

where U_m denotes $(U_1 + U_2)/2\Delta U$. The perturbations, which have the same turbulent intensity profile with the experimental results (Wygnanski and Fiedler, 1970), are the banded white noise as follows:

$$u'(y,z,t) = \sum_{i=1}^{N_f} A\exp(-0.55y^2)\sin\{2\pi f_i t + \phi_i(y,z,f_i)\}, \tag{7}$$

where the range of frequency f_i is set to be $0.034f_0 \leqslant f_i \leqslant 4.13f_0$, and f_0 is the frequency which corresponds to the most unstable wavelength (Λ) for the inlet mean velocity profile. From the mean velocity profile at the inflow boundary, one can estimate the most unstable wavelength by using a linear instability theory. For a hyperbolic tangent profile used in this study, the most unstable wave number is given as $\alpha = 0.4446$ (Michalke, 1964). The wavelength which corresponds to this wave number is $\Lambda = 14.132\delta_{\omega,0}$. Phase ϕ_i is given randomly by using random numbers independent of y, z and f_i. Amplitude A is determined by setting the turbulence intensity at the center of the shear layer to be 2% of the mean velocity difference ΔU. In order to reproduce the realistic inflow boundary condition, "lifetime" of the perturbation is defined. The lifetime is also given by using random numbers independent of y, z and f_i. For instance, suppose one component of perturbations f_1 with lifetime t_1 at a fixed point $(y,z)_{x=0}$. During the period of t_1, phase ϕ_1 of this component is kept. When its lifetime t_1 is over, this component will inflow with a new phase ϕ_2 and has new lifetime t_2. In this way, a realistic velocity inflow boundary condition

is produced. For the velocity outflow boundary condition and the pressure boundary condition, convective-viscous and pressure transport methods developed in our previous study (Miyauchi et al., 1994) are used. The outflow boundary condition used in this study has been verified by changing the length of computational domain in the streamwise direction and shown that the accuracy near the boundary does not degrade (Miyauchi et al., 1994).

In this study, DNS of a spatially-developing mixing layer with the velocity ration $R = (U_1 - U_2)/(U_1 + U_2) = 0.33$ is conducted, and Reynolds number which is based on $\delta_{\omega,0}$ and ΔU at the inlet is 700. The numerical parameters for DNSs of a spatially-developing mixing layer (SML) and a temporally-developing mixing layer (TML) (Tanahashi et al., 2001) are shown in Table 1. The enlarged streamwise region for SML requires more grid points. In general, DNS of various turbulent flows have been conducted with the spatial resolution of $2 \sim 3\eta$. This spatial resolution is determined from lots of DNS of homogeneous isotropic turbulence. In those DNS, the highest wave number, $k_{\max}$ is selected to be $k_{\max}\eta > 1$, which corresponds 3.14η. In this simulation, we also set the spatial resolution to about 3η. Since a spectral method based on sine/cosine series is used in the transverse direction, the distribution of the grid points in this direction is uniform. The number of grid point in this direction is the same with that in the previous DNS of the temporally-developing turbulent mixing layer (Tanahashi et al., 2001). Therefore, the spatial resolution in the transverse direction is enough.

The computational domain is selected to be $30\Lambda \times 6\Lambda \times 8/3\Lambda$. The length in the streamwise direction is selected to be able to capture the second pairing of large-scale structure (Kelvin–Helmholtz roller). The length in the transverse direction is selected to be enough to avoid mirror vortex effects which might be caused by the free-slip boundary condition, and that in the spanwise direction is selected according to the 3/2 instability of the two-dimensional Kelvin–Helmholtz roller (Pierrehumbert and Widnall, 1982).

Table 1
Numerical parameters for DNSs of mixing layers

ID	$Re_{\omega,0}$	$N_x \times N_y \times N_z$	$L_x \times L_y \times L_z$
SML	700	$2160 \times 433 \times 192$	$30\Lambda \times 6\Lambda \times 8/3\Lambda$
TML	700	$288 \times 433 \times 192$	$4\Lambda \times 6\Lambda \times 8/3\Lambda$

3. Statistics of spatially-developing mixing layer

Development of Reynolds number (Re_λ) based on Taylor microscale and rms of velocity fluctuation at the center of shear layer is shown in Fig. 1a. In order to show the difference between spatially- and temporally-developing mix-

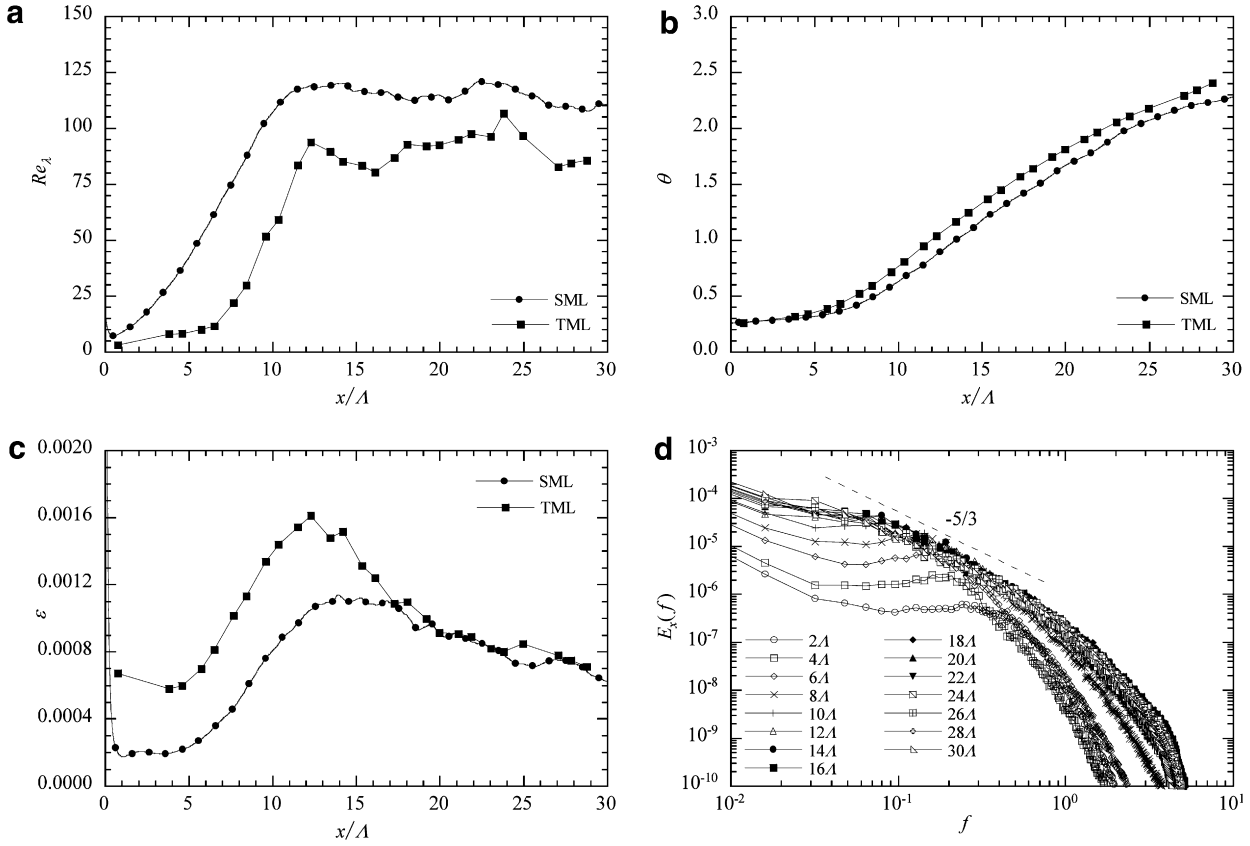

Fig. 1. Statistics of spatially-developing mixing layer. (a) Re_λ at the center of the mixing layer, (b) momentum thickness, (c) energy dissipation rate at the center the shear layer and (d) energy spectra of the streamwise velocity component at shear layer center.

ing layers, the result of temporally-developing mixing layer (Tanahashi et al., 2001) is also shown by converting the time-coordinate into the spatial coordinate based on the Taylor's hypothesis. Although $Re_{\omega,0}$ is the same, the development of Re_λ is quite different. For the temporally-developing mixing layer, Re_λ is low until $x = 8\Lambda$ and increases rapidly from 8Λ to 12Λ. In contrast, for the spatially-developing mixing layer, Re_λ increases linearly until $x = 12\Lambda$. In the downstream region, Re_λ is fluctuating moderately for both cases and the mixing layer is considered to attain fully-developed turbulent state. In such regions, Re_λ of spatially-developing mixing layer is higher than that of the temporally-developing mixing layer. These results suggest that the laminar–turbulent transition process and the fully-developed state are significantly affected by the feedback of downstream information.

Momentum thickness (θ) is frequently used to evaluate the growth rate of mixing layers. θ is defined by

$$\theta = \int_{-L_y/2}^{L_y/2} (U_1 - U(y))(U(y) - U_2)\mathrm{d}y, \tag{8}$$

where U_1 and U_2 represent the mean velocities of the high-speed side and low-speed side, respectively. Fig. 1b shows the development of θ for spatially- and temporally-developing mixing layers. Although θ increases linearly until $x \approx 8\Lambda$ for both cases, it is thinner for the spatially-developing mixing layer in the upstream region. It can be considered that, for the temporally-developing mixing layer, the large-scale structure driven by Kelvin–Helmholtz instability will grow faster because the flow field is perfectly approximated by a two-dimensional parallel flow. In addition, from the statistics of temporally-developing mixing layer for different $Re_{\omega,0}$, it is shown that the higher Re_λ cases show lower momentum thickness (Tanahashi et al., 2001). According to this result, in the present study, the higher Re_λ of spatially-developing mixing layer might be caused by its lower momentum thickness compared with that of the temporal case.

Fig. 1c shows the development of turbulent energy dissipation rate (ε) at the center of the shear layer. In the upstream region, the value of ε is higher for the temporal case. The peak of ε is observed at $12\Lambda \lesssim x \lesssim 14\Lambda$ for both cases and this position can be considered to the onset of laminar–turbulent transition. In the downstream region where the mixing layer is fully-developed, energy dissipation rates of both cases coincide very well and decrease moderately. These results reflect self-similarity of turbulent mixing layer.

In Fig. 1d, energy spectra of the streamwise velocity at the center of shear layer are shown for the present spatially-developing case. The energy spectra show that DNS in the present study well resolved the velocity fluctuation in small scales. The development of the energy spectrum suggests that velocity fluctuations in high frequency increase as the flow goes into the downstream. It has been reported that the energy spectrum shows a slope of $-5/3$ in the relatively low frequency range in the fully-developed turbulent mixing layer (Comte et al., 1992; Rogers and Moser, 1994). Fig. 1d shows that spectra in the downstream regions also show a $-5/3$ power law in the low frequency range. This power law also suggests that flow attained fully-developed state in those regions.

4. Visualization of coherent fine scale eddies

Fig. 2 shows iso-surfaces of the pressure with a negative threshold ($p = -0.05$). The large-scale structures are visualized very clearly by the low-pressure region. The process of roll-up, first pairing and second pairing of the well-known Kelvin–Helmholtz structures, can be observed in $5\Lambda \lesssim x \lesssim 8\Lambda$, $8\Lambda \lesssim x \lesssim 16\Lambda$ and $16\Lambda \lesssim x \lesssim 30\Lambda$, respectively.

The iso-surfaces of the second invariant of velocity gradient tensor (Q), which have been used for the visualization of small-scale structures, are shown in Fig. 3. Note that distinct large Kelvin–Helmholtz rollers cannot be visualized by the second invariant of velocity gradient tensor because rotation rate of those is lower than that of streamwise vortices (rib structures) or fine scale eddies. Due to the Kelvin–Helmholtz instability, large-scale roller structures roll-up and merge into larger structures, and lots of tube-like fine

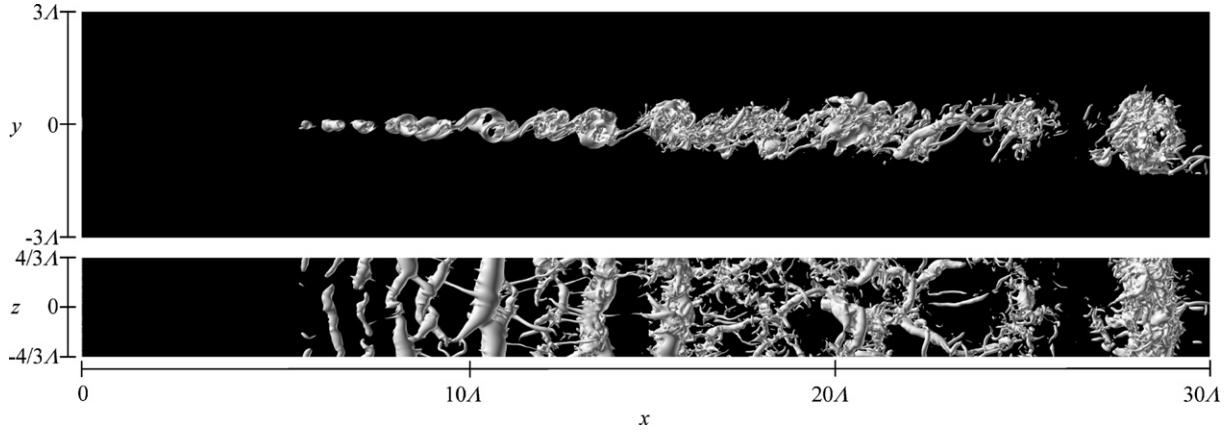

Fig. 2. Iso-surfaces of pressure at $p = -0.05$.

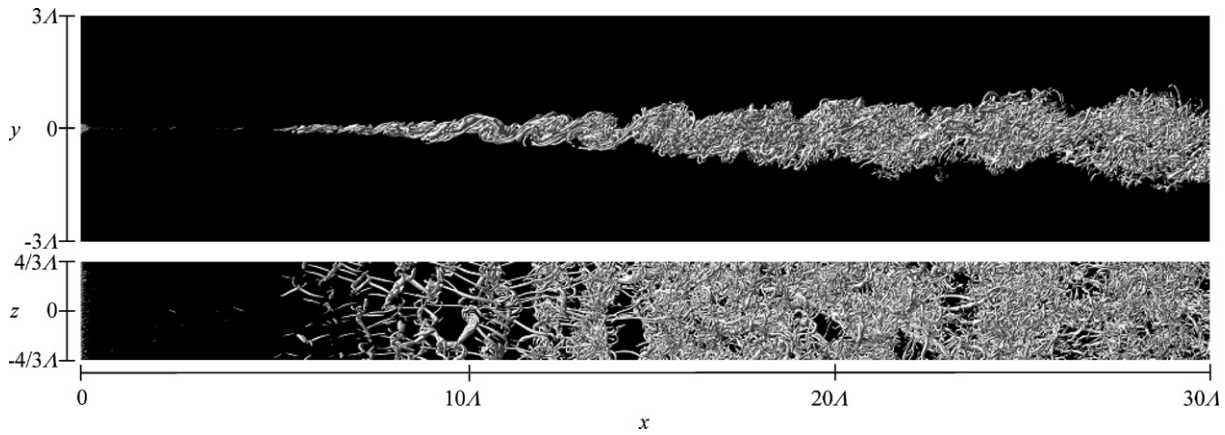

Fig. 3. Iso-surfaces of the second invariant of the velocity gradient tensor at $Q = 0.15$.

scale structures appear simultaneously. In the downstream region, the observed diameters of the tube-like structures become small and their number density becomes high. In addition, from the iso-surfaces of the pressure, several rib vortices are observed in the upstream braid region, while the rib vortices disappear in the downstream braid region. It is indicated that the intensity of rib vortices becomes weak in the process of the transition. In the downstream, however, streamwise structures that are composed of many fine scale tube-like eddies still exist in the braid region. This kind of structure can be thought as traces of the rib vortex in the fully-developed state.

It should be emphasized that iso-surfaces in Figs. 2 and 3 are only used for visualization which makes it possible to grasp an overview of the flow field. In this study, in order to investigate the modification of coherent fine scale eddies in the laminar–turbulent transition in more detail, the rotation axes of the coherent fine scale eddies are extracted by using an axis tracing method (Tanahashi et al., 1999, 2004). The identification scheme consists of the following steps:

(a) Evaluation of Q at each collocation point from the results of DNS.
(b) Probability of existence of positive local maximum of Q near the collocation points is evaluated at each collocation point from Q distribution. Because the case that a local maximum of Q coincides with a collocation point is very rare, it is necessary to define probability on collocation points.
(c) Collocation points with non-zero probability are selected to survey actual maxima of Q. Locations of maximal Q are determined within the accuracy of 10^{-6} by applying a three-dimensional fourth-order Lagrange interpolation to DNS data.
(d) A cylindrical coordinate system (r, θ, z) is considered by setting the maximal point as the origin. The coordinate system is assumed to have advection velocity at the origin. The z-direction is selected to be parallel to the vorticity vector at the maximal point. The velocity vectors are projected on this coordinate and azimuthal velocity u_θ is calculated.
(e) Point that has small variance in azimuthal velocity compared with surroundings is determined. If the azimuthal velocities at $r = 1/5$ computational grid width show same sign for all θ, that point is identified as the center of the swirling motion.
(f) Statistical properties are calculated around the point.
(g) Steps (d)–(f) are conducted for all points determined in step (c).
From (a)–(g) steps, the center of swirling motion ($\boldsymbol{x}_s$) is identified on the cross-section with Q maxima on the axis of the eddy. From $\boldsymbol{x}_s$, axes of each coherent fine scale eddy are searched by using a following auto-tracing algorithm.
(h) From $\boldsymbol{x}_s$, the investigated point is moved in the axial direction with short distance $|\boldsymbol{ds}|$. $\boldsymbol{ds}$ is parallel to the vorticity vector at $\boldsymbol{x}_s$. A new cylindrical coordinate system (r', θ', z') is considered by setting the new point as the origin. On the (r', θ') plane with $z' = 0$, the point with maximum Q is determined, and the steps (c)–(e) are applied.
(i) Rotation axis is determined by repeating the step (h). In this procedure, $|\boldsymbol{ds}|$ is set equal to 1/5 computational grid width. If angle (ϕ_n) between $(\boldsymbol{x}_n - \boldsymbol{x}_{n-1})$ and vorticity vector at $\boldsymbol{x}_{n-1}$ is greater than 30°, the step (h) is applied again with $|\boldsymbol{ds}'| = |\boldsymbol{ds}|\cos(\phi_n)$.
(j) After the calculation of statistical properties, above steps are repeated until second invariant on the axis becomes negative or swirling motion cannot be detected.
(k) Steps (h)–(j) are conducted in the opposite direction of vorticity vector at $\boldsymbol{x}_s$.
(l) Steps (h)–(k) are applied for the next starting point.

Figs. 4 and 5 show distributions of rotation axes of coherent fine scale eddies in domains from 10Λ to 22Λ and from 22Λ to 30Λ, respectively. Here, the diameter of axis is drawn to be proportional to square root of Q on the axis. Thicker axis represents strong rotation rate of the eddy and finer axis does weak one. In the early stage of the transition to turbulence (Fig. 4), the rib vortices appearing in braid regions show quite high Q and the roller

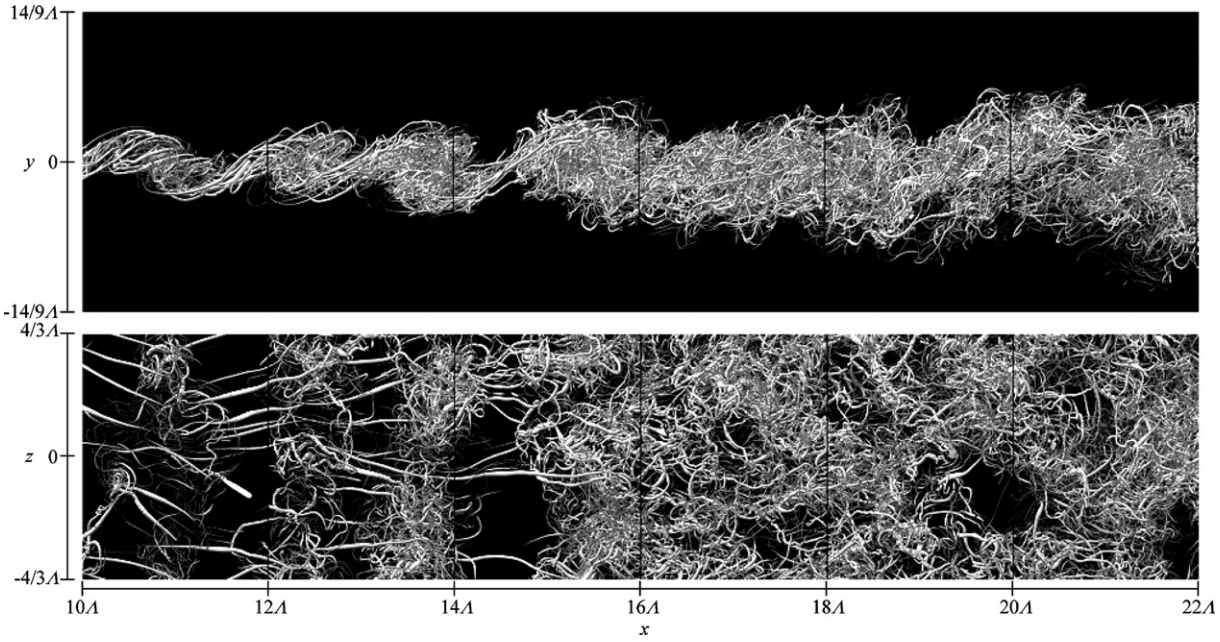

Fig. 4. Spatial distributions of rotation axes of coherent fine scale eddy in the process of the laminar–turbulent transition ($10 \leqslant x/\Lambda \leqslant 22$).

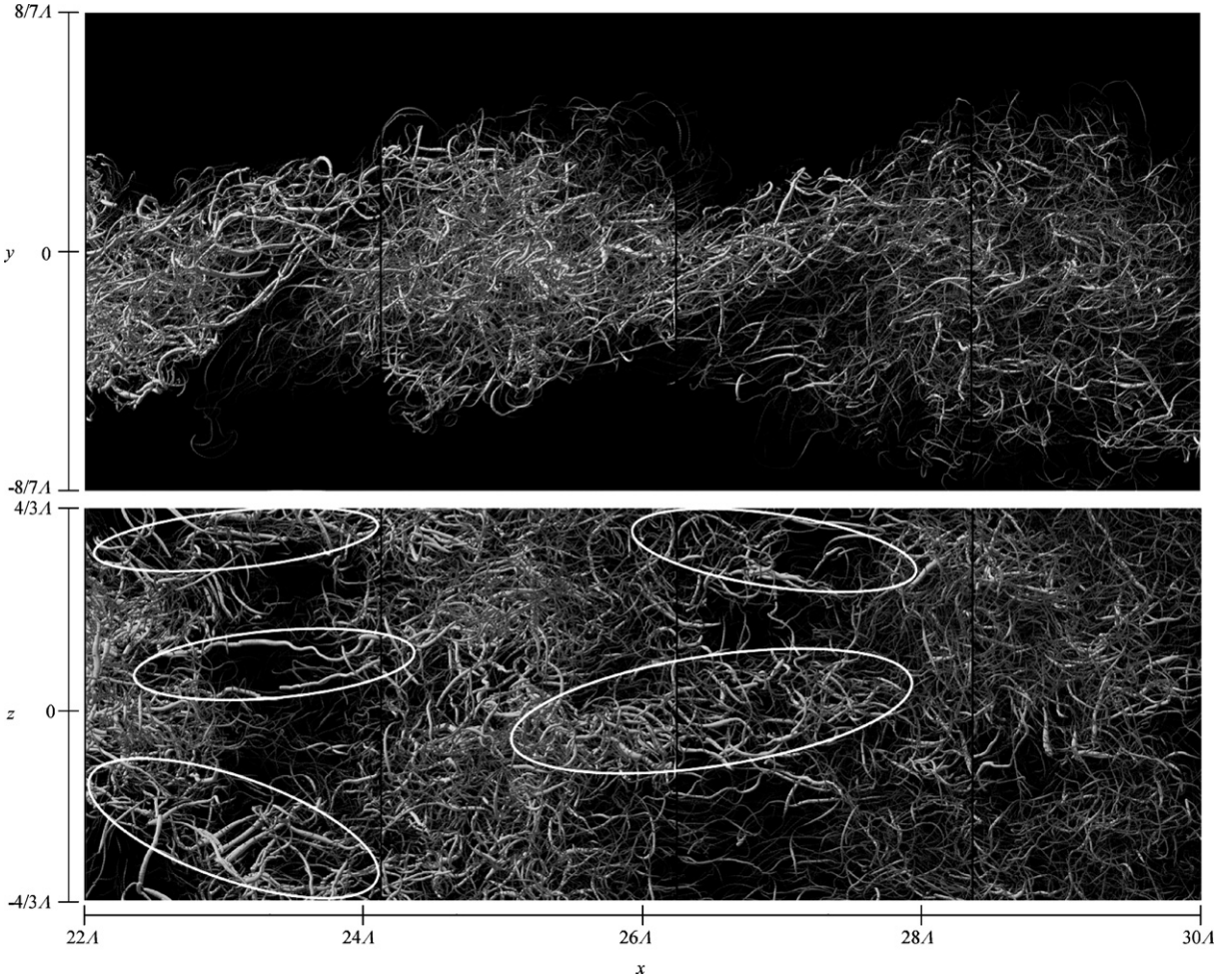

Fig. 5. Spatial distributions of rotation axes of coherent fine scale eddy in the fully-developed region ($22 \leqslant x/\Lambda \leqslant 30$).

structures are composed of coherent fine scale eddies with low Q. As the laminar–turbulent transition is proceeded by interactions between rib vortices and the roller structures, coherent fine scale eddies with high Q can be found in the roller structure and rib vortices become relatively weak. In the fully-developed region (Fig. 5), not only the large-scale rollers, but also the rib-like structures (denoted by white circles) are composed of the coherent fine scale structures. Even in the fully-developed state, the portion of coherent fine scale eddies with high Q is qualitatively high in the rib-like structure compared with that in the roller structure. This fact means that distinctions between roller structure and rib-like structure do not disappear during the laminar–turbulent transition and still exist in the fully-developed turbulent state from the view point of fine scale structure.

5. Laminar–turbulent transition and coherent fine scale eddies

In this study, centers of coherent fine scale eddies are extracted by using the eddy identification scheme which was used in our previous studies (Tanahashi et al., 1996, 1997b). The vortex center is defined as a point with the maximum second invariant of the velocity gradient tensor on the axis of a single eddy. Therefore, one tube-like eddy has one vortex center.

5.1. Scaling law of coherent fine scale eddies

Fig. 6 shows the probability density functions (pdf) of diameters of coherent fine scale eddies. The diameters are normalized by Kolmogorov length scale which is calculated at the center of the shear layer in each region. The most expected diameter is almost constant and is 8η in the transition process. This diameter in the transition process is consistent with that obtained in fully-developed turbulent flows except for the near-wall eddy (Tanahashi et al., 2004). The probability density of the coherent fine scale eddies with large diameters decreases with the development of the flow field. The pdfs of the maximum azimuthal velocity of coherent fine scale eddies is shown in Fig. 7. The maximum azimuthal velocity is normalized by Kolmogorov velocity. The most expected maximum azimuthal velocity decreases from $2.0u_k$ to $1.2u_k$ during the transition. Similar to the diameter, the probability density of the coherent fine scale eddies with large azimuthal velocity also decreases through the transition. It has been clarified that the most expected maximum azimuthal velocity in fully-developed turbulent flows is $1.2u_k$ (Tanahashi et al., 2001, 2004). The behavior of the maximum azimuthal velocity in the transition process shows that fine scale eddy in the transition is stronger than that in the fully-developed state.

5.2. Anisotropy of mixing layer

In our previous study (Tanahashi et al., 1997b), the anisotropic feature of mixing layer in the fully-developed state has been discussed based on the directional dependence of the coherent fine scale eddies. In the present study, the characteristics of the anisotropic feature in the laminar–turbulent transition are investigated. To investigate directional dependence of the fine scale eddy, the inclination angle of rotating axis of a eddy with respect to the mean shear direction is defined as follows:

$$\cos\theta_0 = \frac{\boldsymbol{\omega}_c \cdot \boldsymbol{e}_\omega}{|\boldsymbol{\omega}_c| \cdot |\boldsymbol{e}_\omega|}, \tag{9}$$

where $\boldsymbol{\omega}_c$ and $\boldsymbol{e}_\omega$ represent vorticity vector at the center of a coherent fine scale eddy and the direction of mean vorticity vector ($\boldsymbol{e}_\omega = (0,0,-1)$) in mixing layer, respectively. The value of $\cos\theta_0$ will be 1 if fine scale eddies are co-rotating with large-scale structure (Kelvin–Helmholtz roller), and will be -1 if they are counter-rotating. Here, if the rotating axes of the fine scale eddies have a fully random distribution, probability density for all $\cos\theta_0$ will become 0.5.

Fig. 8 shows pdfs of inclination angles. The positive gradients of the pdfs with respect to $\cos\theta_0$ indicate that number of co-rotating eddies is larger than that of counter-rotating ones. In the early stage of the transition, the probability density of counter-rotating eddies is very low. The

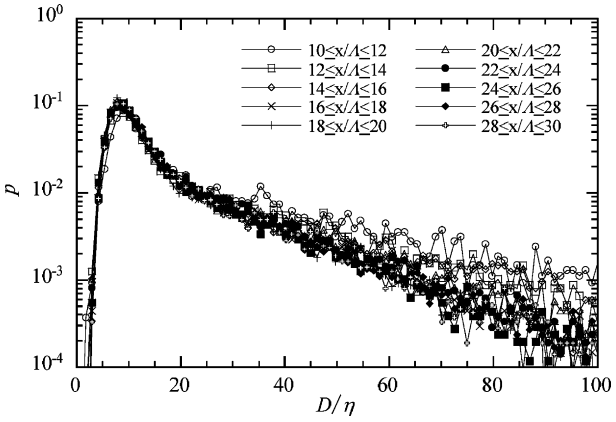

Fig. 6. Pdfs of the diameter of coherent fine scale eddies.

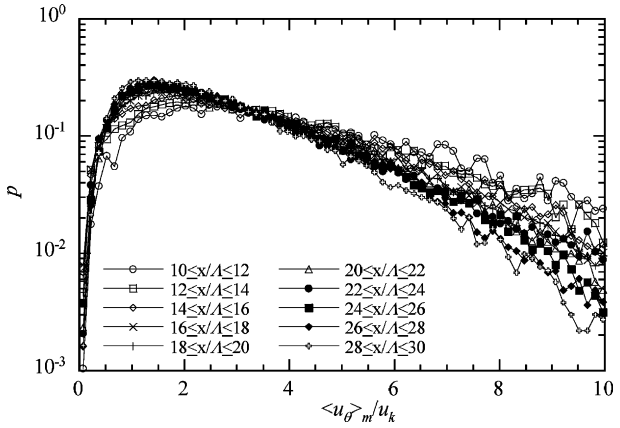

Fig. 7. Pdfs of maximum azimuthal velocity of coherent fine scale eddies.

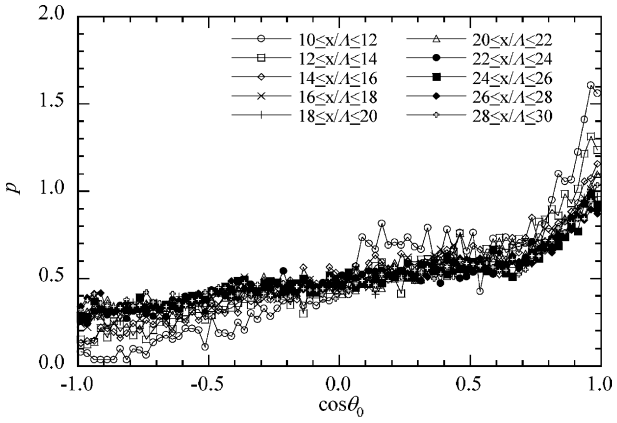

Fig. 8. Pdfs of $\cos\theta_0$ of coherent fine scale eddies.

counter-rotating eddies appear in the transition process, which is consistent with the observations reported by Moser and Rogers (1991) and Comte et al. (1992). It should be noted that the probability density of the eddies with $\cos\theta_0 \approx 0.25$ is relatively high in the early stage of the transition. This phenomenon is attributed to the existence of the rib vortex. To show it more clearly, Fig. 9 shows the distributions of the vorticity vectors on the rotating axes of coherent fine scale eddies for the early stage of the transition and the fully-developed region, respectively. In the early stage of the transition, there are many single rib vortices obviously in the braid region. Their inclination angles are about 75° ($\cos 75° \approx 0.25$). In the fully-developed region, this kind of rib vortices does not exist. In this region, rib-like structures consist of many fine scale eddies as shown in Fig. 5.

5.3. Strain rate at the center of coherent fine scale eddy

In this section, strain rate acting on the coherent fine scale eddy is investigated by evaluating the strain rate tensor S_{ij} at the center of the coherent fine scale eddy. Fig. 10 shows the definition of eigenvalues and angles between the vorticity vector and eigenvectors at the center of a coherent fine scale eddy. Here, α, β and γ are the minimum, intermediate and maximum eigenvalues of S_{ij}, respectively. For the incompressible flow, eigenvalues are satisfying $\alpha+\beta+\gamma=0$. The eigenvectors corresponding to α, β and γ are represented by $\boldsymbol{e}_1$, $\boldsymbol{e}_2$ and $\boldsymbol{e}_3$. The angles between $\boldsymbol{\omega}_c$ and $\boldsymbol{e}_1$, $\boldsymbol{e}_2$ and $\boldsymbol{e}_3$ are denoted by θ, ψ and ϕ.

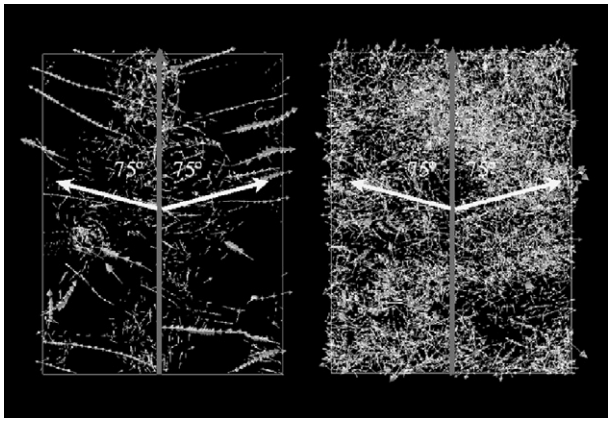

Fig. 9. Vorticity vectors on the rotation axis of coherent fine scale eddies of the braid region in early stage of transition (left: $10 \leqslant x/\Lambda \leqslant 12$, $-4/3 \leqslant z/\Lambda \leqslant 4/3$) and in fully-developed state (right: $16 \leqslant x/\Lambda \leqslant 18$, $-4/3 \leqslant z/\Lambda \leqslant 4/3$).

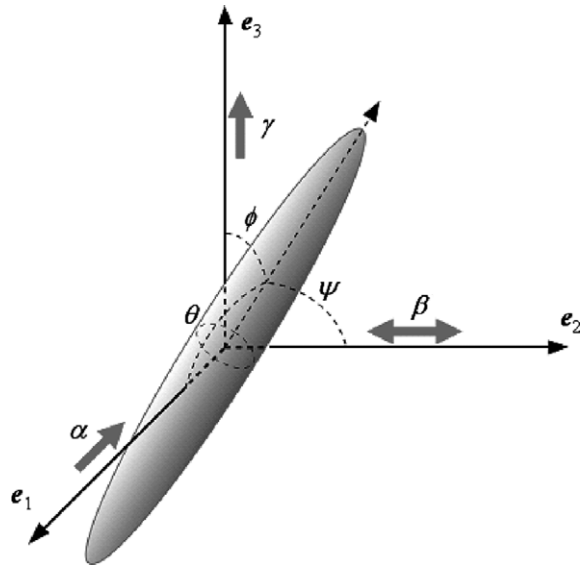

Fig. 10. Schematic of the definitions of the eigenvectors and eigenvalues at the center of the eddy.

Figs. 11–13 show pdfs of the eigenvalues at the center of the coherent fine scale eddy. The eigenvalues are normalized by the reciprocal of the Kolmogorov time scale ($=u_k/\eta$) at the center of the mixing layer in each region. In the process of the transition to turbulence, probability densities of eigenvalues with large absolute values decrease, while those with small absolute values increase. It is indicated that the strain rate acting on the center of coherent fine scale eddy becomes weak as the flow transits to turbulence.

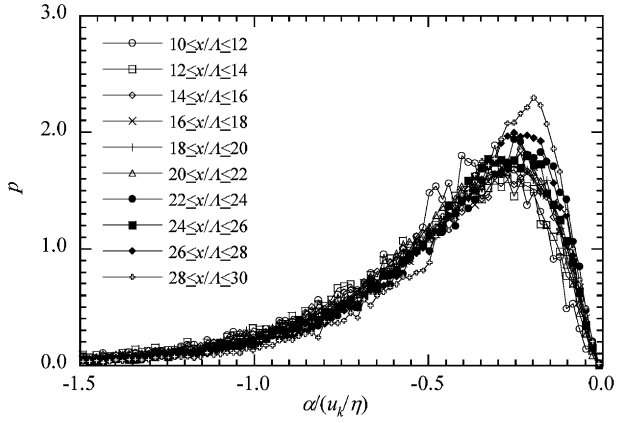

Fig. 11. Pdfs of the minimum eigenvalue α at the center of coherent fine scale eddy.

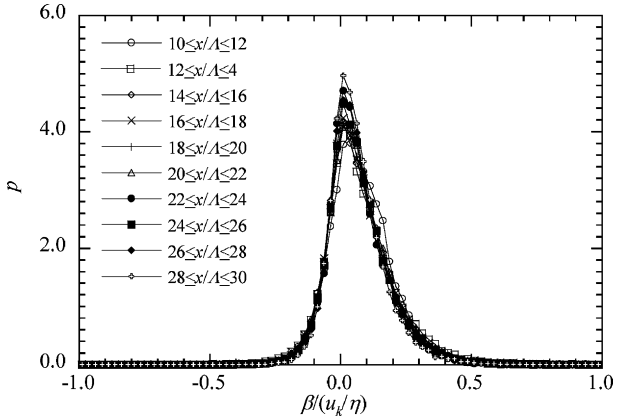

Fig. 12. Pdfs of the intermediate eigenvalue β at the center of coherent fine scale eddy.

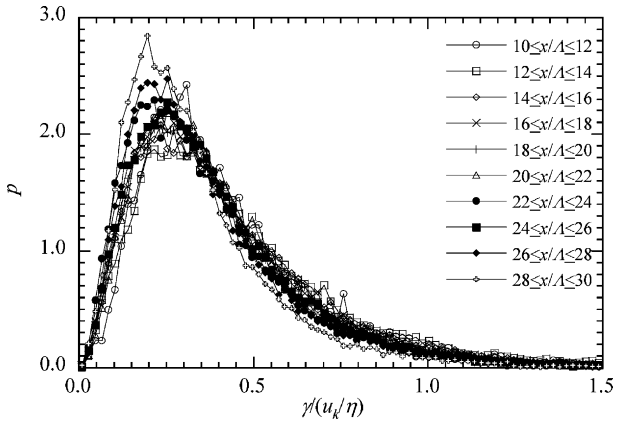

Fig. 13. Pdfs of the maximum eigenvalue γ at the center of coherent fine scale eddy.

In our previous study (Tanahashi et al., 2001), it has been clarified that the most expected eigenvalue ratio at the center of the coherent fine scale eddy is $\alpha{:}\beta{:}\gamma = -5{:}1{:}4$ and is different from that in high dissipation rate region ($-4{:}1{:}3$) (Soria et al., 1994). In this study, a following modified eigenvalue ratio σ is introduced:

$$\sigma = \frac{\gamma - \beta}{\gamma + \beta}. \tag{10}$$

A similar eigenvalue ratio has been introduced to discuss characteristics of a stretched vortex under asymmetric strain fields (Moffatt et al., 1994). However, in this study, σ is defined by using β and γ due to characteristics of the coherent fine scale eddy instead of α and β which have been used by Moffatt et al. (1994). According to Eq. (10), the coherent fine scale eddies are stretched in the direction of the intermediate eigenvalue for $0 < \sigma < 1$ and are compressed from that direction for $1 < \sigma < 3$. Pdfs of the modified eigenvalue ratio are shown in Fig. 14. In the transition process, the shapes of the pdfs coincide very well and the most expected eigenvalue ratio is constant (=0.6). Most of the coherent fine scale eddies are in the range of

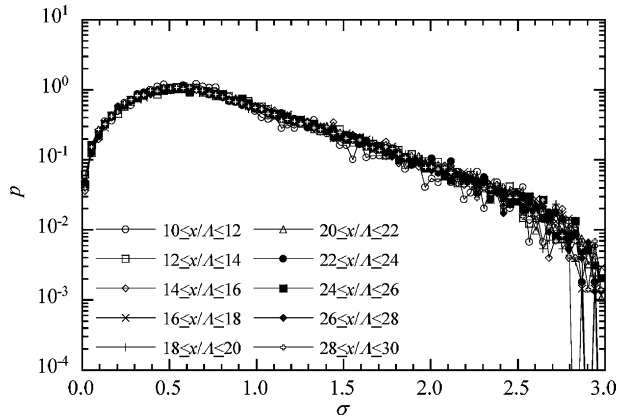

Fig. 14. Pdfs of the eigenvalue ratio at the center of coherent fine scale eddy.

$0 < \sigma < 1$, and are stretched in the direction of the intermediate eigenvalue. In contrast, eddies which are compressed in this direction are very few. Since the modified eigenvalue ratio shows a peak at $\sigma = 0.6$, the most expected eigenvalue ratio becomes $\alpha{:}\beta{:}\gamma = -5{:}1{:}4$ which coincides with that in fully-developed turbulence (Tanahashi et al., 2001, 2004). The results of eigenvalues and eigenvalue ratio in the process of the transition show that the most expected eigenvalue ratio is sustained to be constant. However, the magnitude of the strain rate decreases in the transition process and approaches to that in the fully-developed turbulence.

In addition to these characteristics, Miyauchi et al. (2002) and Kang et al. (2006) have investigated structures of the coherent fine scale eddy on the plane perpendicular to the axis by introducing a phase average analysis. Since the azimuthal velocity near the center of the eddy is dominated by $k_\theta = 2$ mode, phase averages are conducted based on the phase of $k_\theta = 2$ for various quantities around the eddy. Here, k_θ denotes wave number in the azimuthal direction. Figs. 15 and 16 show phase-averaged distribution of velocity vector and energy dissipation rate on the plane perpendicular to the axis of coherent fine scale eddy. Energy dissipation rate on each plane is normalized by using the value at the center. As shown by our previous

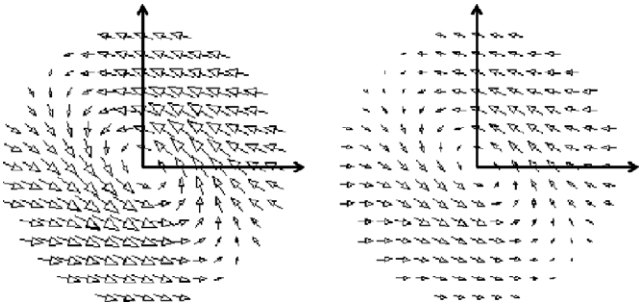

Fig. 15. Phase-averaged distribution of velocity vector on the plane perpendicular to the axis of coherent fine scale eddy for $10 \leqslant x/\Lambda \leqslant 12$ (left) and $28 \leqslant x/\Lambda \leqslant 30$ (right).

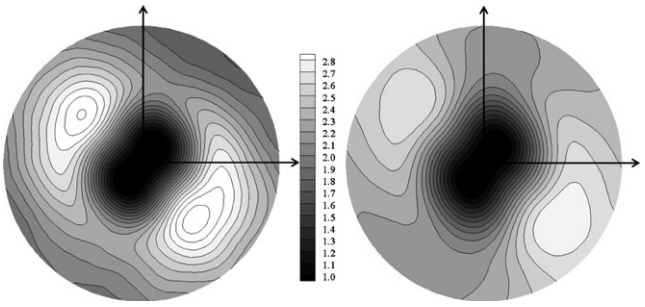

Fig. 16. Phase-averaged distribution of energy dissipation rate on the plane perpendicular to the axis of coherent fine scale eddy for $10 \leqslant x/\Lambda \leqslant 12$ (left) and $28 \leqslant x/\Lambda \leqslant 30$ (right).

studies (Miyauchi et al., 2002; Kang et al., 2006), the coherent fine scale eddy shows elliptic feature on its cross-section. Figs. 15 shows that, in the early stage of transition ($10 \leqslant x/\Lambda \leqslant 12$), the coherent fine scale eddy is rotating with a high speed, while, in the fully-developed state ($28 \leqslant x/\Lambda \leqslant 30$), the rotation speed decreases. This phenomenon is consistent with the result that the most expected maximum azimuthal velocity of coherent fine scale eddies becomes slow during the laminar–turbulent transition. As rotation rate of the coherent fine scale eddy and strain rate acting on the eddy become weak, energy dissipation rate is also found to become low with the transition to turbulence as shown in Fig. 16.

6. Conclusions

In this study, relations between the coherent fine scale eddy and laminar–turbulent transition are investigated in a spatially-developing mixing layer by using direct numerical simulation at relatively high Reynolds number.

By using the axis tracing method, all of the coherent fine scale eddies existing in the flow field are extracted without any thresholds. Not only the spatial distributions, but also the intensity of the fine scale structures were clearly represented. The result of visualizations shows that large-scale roller and rib vortex interact with each other and the transition occurs, which results in the appearance of numerous coherent fine scale eddies. In the fully-developed state, the large-scale roller and rib structure are still observed and the rib structure is composed of lots of coherent fine scale eddies instead of a single eddy observed in the early stage of the transition.

In the process of the transition, the most expected diameter of the coherent fine scale eddies is maintained to be 8η, while the most expected maximum azimuthal velocity of those decreases. In addition, the probability density of coherent fine scale eddies with large diameter or large maximum azimuthal velocity decreases with the transition.

It is shown that anisotropic features of the turbulent mixing layer can be explained by the spatial distribution of coherent fine scale eddies. In the transition process, number of co-rotating eddies with large-scale structure is greater than that of counter-rotating ones.

With the transition to turbulence, the strain rate acting on the center of coherent fine scale eddy tends to become weak, whereas the most expected eigenvalue ratio is maintained to be $\alpha{:}\beta{:}\gamma = -5{:}1{:}4$. As the strain rate decreases, the energy dissipation rate on the major axis of coherent fine scale eddies becomes low in the transition process.

Acknowledgments

This work is partially supported by Grant-in-Aid for the Scientific Research (A) (No. 15206023) and (S) (No. 18106004) of Japan Society for Promotion of Science.

References

Comte, P., Lesieur, M., Lamballais, E., 1992. Large- and small-scale stirring of vorticity and passive scalar in a 3-D temporal mixing layer. Phys. Fluids A 4, 2761–2778.

Jimenez, J., Wray, A.A., Saffman, P.G., Rogallo, R.S., 1993. The structure of intense vorticity in isotropic turbulence. J. Fluid Mech. 255, 65–90.

Kang, S.-J., Tanahashi, M., Miyauchi, T., 2006. Elliptic feature of coherent fine scale eddies in turbulent channel flows. J. Mech. Sci. Technol. 20, 262–270.

Lundgren, T.S., 1982. Strained spiral vortex model for turbulent fine structure. Phys. Fluids 25, 2193–2203.

Michalke, A., 1964. On the inviscid instability of the hyperbolic tangent velocity profile. J. Fluid Mech. 19, 543–556.

Miyauchi, T., Tanahashi, M., Suzuki, M., 1994. Inflow and outflow boundary conditions for direct numerical simulations. JSME Int. J. 60B, 813–821.

Miyauchi, T., Tanahashi, M., Matsuoka, K., 1996. Localized upwind scheme for DNS of turbulence. In: Proc. 10th Symp. on Computational Fluid Dynamics, pp. 122–123.

Miyauchi, T., Tanahashi, M., Takata, N., Iwase, S., 2002. Scalar dissipation rate and coherent fine scale eddies in turbulence. In: Int. Symp. on Dynamics and Statistics of Coherent Structures in Turbulence, pp. 249–258.

Moffatt, H.K., Kida, S., Ohkitani, K., 1994. Stretched vortices – the sinews of turbulence; large-Reynolds-number asymptotics. J. Fluid Mech. 259, 241–264.

Moser, R.D., Rogers, M.M., 1991. Mixing transition and the cascade to small scales in a plane mixing layer. Phys. Fluids A 3, 1128–1134.

Moser, R.D., Rogers, M.M., 1993. The three-dimensional evolution of a plane mixing layer: paring and transition to turbulence. J. Fluid Mech. 247, 275–320.

Pierrehumbert, R.T., Widnall, S.E., 1982. The two- and three-dimensional instabilities of a spatially periodic shear layer. J. Fluid Mech. 114, 59–82.

Pullin, D.I., Saffman, P.G., 1993. On the Lundgren–Townsend model of turbulent fine scales. Phys. Fluids A 5, 126–145.

Rogers, M.M., Moser, R.D., 1994. Direct numerical simulation of a self-similar turbulent mixing layer. Phys. Fluids 6, 903–923.

She, Z.-S., Jackson, E., Orszag, S.A., 1990. Intermittent vortex structures in homogeneous isotropic turbulence. Nature 344, 226–228.

Soria, J., Soudergaard, R., Cantwell, B.J., Chong, M.S., Perry, A.E., 1994. Study of the fine-scale motions of incompressible time-developing mixing layers. Phys. Fluids A 6, 871–884.

Tanahashi, M., Miyauchi, T., 1995. Small scale eddies in turbulent mixing layer. In: Proc. 10th Symp. Turbulent Shear Flows vol. 1, pp. 1-79–1-84.

Tanahashi, M., Miyauchi, T., Yoshida, T., 1996. Characteristics of small scale vortices related to turbulent energy dissipation. In: Transport Phenom. Thermal-Fluid Eng. 2, pp. 1256–1261.

Tanahashi, M., Miyauchi, T., Matsuoka, K., 1997a. Coherent fine scale structures in turbulent mixing layers. In: Proc. Turbulence, Heat Mass Transfer 2, pp. 451–470.

Tanahashi, M., Miyauchi, T., Ikeda, J., 1997b. Scaling law of coherent fine scale structure in homogeneous isotropic turbulence. In: Proc. 11th Symp. Turbulent Shear Flow, vol. 1, pp. 4-17–4-22.

Tanahashi, M., Iwase, S., Uddin, A.Md., Miyauchi, T., 1999. Three-dimensional features of coherent fine scale eddies in turbulence. In: Proc. Turbulence and Shear Flow Phenomena 1, pp. 79–84.

Tanahashi, M., Iwase, S., Miyauchi, T., 2001. Appearance and alignment with strain rate of coherent fine scale eddies in turbulent mixing layer. J. Turbulence 2, 17.

Tanahashi, M., Kang, S.-J., Miyamoto, T., Shiokawa, S., Miyauchi, T., 2004. Scaling saw of fine scale eddies in turbulent channel flows up to $Re_\tau = 800$. Int. J. Heat Fluid Flow 25, 331–340.

Tennekes, H., 1968. Simple model for the small-scale structure of turbulence. Phys. Fluids 11, 669–671.

Townsend, A.A., 1951. On the fine-scale structure of turbulence. Proc. Roy. Soc. A 208, 534–542.

Vincent, A., Meneguzzi, M., 1991. The spatial structure and statistical properties of homogeneous turbulence. J. Fluid Mech. 225, 1–25.

Wygnanski, I., Fiedler, H.E., 1970. The two-dimensional mixing region. J. Fluid Mech. 41, 327–361.